

and the contacts with specific guanine residues within sites I and II lead us to predict that different proteins interact with these sites. Site II encompasses a TATA box and, unlike site I, contains interactions with guanine residues on both strands. The specific G contacts in site II can be visualized as part of a region with partial dyad symmetry (as shown below) with the insertion of a T·A base pair on the 5' side of the dyad.



In addition, the central sequence GGTC has been shown to be specific for histone genes (17). The 5' portion of site II includes two additional guanine contacts on the upper strand that are centered about the sequence GCTTTCGGTTTC, containing an imperfect hexanucleotide repeat. These two other guanine contacts and the large size of the DNase I footprint indicate that more than one protein interacts at site II. A functional role for site II is suggested by the requirement for the entire site in order to support correctly initiated transcription when deletion mutants were assayed in vivo (12). Interestingly, only the 3' segment of site II is necessary for properly initiated transcripts in whole cell extracts (18) or in nuclear extracts (19).

In the case of the 3' portion of site I, the sequence around position -125 includes a region with similarity to the Sp1 decanucleotide consensus $\begin{matrix} G & G & G & G & C & G & G & G & C \\ T & A & G & G & T & A & A & T \end{matrix}$ (20). In addition the G contacts we detect in this region on the upper strand are similar to those for three tandem Sp1 binding sites in the HTLV-III retroviral promoter (21). However, we do not see the tandem arrangement of Sp1 sites characteristic of viral promoters in this H4 histone gene (22). In the 5' portion of site I, we see two additional G contacts in a region containing a direct hexanucleotide repeat GAAATGACGAAATG; these contacts occur symmetrically around a central AC dinucleotide. A gel retardation assay provides evidence that sequences in the 5' portion of site I are able to bind to a protein (HiNF-A) fractionated from HeLa nuclear extracts (23). The Taq I site at -133 is also highly accessible to restriction endonuclease digestion in nuclei, further evidence of the potential for interaction of two different proteins with site I. If the protein interacting with the 3' portion of site I is Sp1, this would be the first demonstration of Sp1 binding in vivo. Our results are consistent with the potential for binding of at least four proteins to the two sites detected in vivo.

We have interpreted our results within the

context of the types of sequences that most likely contribute to transcription of this cell cycle-regulated human H4 histone gene in vivo. Because these protein-DNA interactions persist throughout the cell cycle, we suggest that these complexes contribute to the basal level of transcription, which occurs during G₁, S, G₂, and mitosis (16, 24). These results do not provide a direct explanation for the enhanced transcription of this H4 histone gene in early S phase (4, 16). However, it is possible that these protein-DNA interactions, detected throughout the cell cycle, may serve as contact points for factors that are responsible for the cell cycle-specific fluctuations in transcription of this gene. Alternatively, specific protein-DNA interactions may be found in a more upstream or in a more downstream region than we have investigated.

REFERENCES AND NOTES

1. F. Sierra *et al.*, *Proc. Natl. Acad. Sci. U.S.A.* **79**, 1795 (1982).
2. N. Heintz, M. Zernik, R. G. Roeder, *Cell* **24**, 661 (1981).
3. G. S. Stein *et al.*, in *Recombinant DNA and Cell Proliferation*, G. S. Stein and J. L. Stein, Eds. (Academic Press, New York, 1984), pp. 107-143.
4. M. Plumb, J. Stein, G. Stein, *Nucleic Acids Res.* **11**, 2391 (1983).
5. M. Artshesky, A. M. Delegeane, A. S. Lee, *Mol. Cell. Biol.* **4**, 2364 (1984).
6. S. Chrysogelos, D. E. Riley, G. Stein, J. Stein, *Proc. Natl. Acad. Sci. U.S.A.* **82**, 7535 (1985).
7. M. L. Moreno, S. A. Chrysogelos, G. S. Stein, J. L. Stein, *Biochemistry* **25**, 5364 (1986).
8. L. Green *et al.*, *Proc. Natl. Acad. Sci. U.S.A.* **83**, 2315 (1986).
9. O. Capasso and N. Heintz, *ibid.* **82**, 5622 (1985).
10. H. L. Sive, N. Heintz, R. G. Roeder, *Mol. Cell. Biol.* **6**, 3329 (1986).
11. L. Dailey, S. M. Hanly, R. G. Roeder, N. Heintz, *Proc. Natl. Acad. Sci. U.S.A.* **83**, 7241 (1986).
12. P. Kroeger *et al.*, *ibid.*, in press.
13. G. M. Church and W. Gilbert, *ibid.* **81**, 1991 (1984).
14. A. Ephrussi, G. M. Church, S. Tonegawa, W. Gilbert, *Science* **227**, 134 (1985).
15. K. Zinn and T. Maniatis, *Cell* **45**, 611 (1986).
16. L. Baumbach, G. S. Stein, J. L. Stein, *Biochemistry*, in press.
17. C. C. Hentschel and M. L. Birnstiel, *Cell* **25**, 301 (1981).
18. F. Sierra, G. Stein, J. Stein, *Nucleic Acids Res.* **11**, 7069 (1983).
19. K. Wright, personal communication.
20. M. R. Briggs, J. T. Kadonaga, S. P. Bell, R. Tjian, *Science* **234**, 47 (1986).
21. K. A. Jones, J. T. Kadonaga, P. A. Luciw, R. Tjian, *ibid.* **232**, 755 (1986).
22. D. Gidoni *et al.*, *ibid.* **230**, 511 (1985).
23. A. J. van Wijnen, J. L. Stein, G. S. Stein, *Nucleic Acids Res.* **15**, 1679 (1987).
24. N. Heintz, H. L. Sive, R. G. Roeder, *Mol. Cell. Biol.* **3**, 539 (1983).

Supported by grants from NIH (GM32010), NSF (PCM83-18177), the March of Dimes Birth Defects Foundation (1-813), and by a postdoctoral fellowship of the Swiss National Foundation (U.P.). We thank H. Ostrer, P. Laipis, G. Zambetti, A. van Wijnen, and K. Wright for critically reading the manuscript.

5 January 1987; accepted 3 April 1987

The Dynamics of Free Calcium in Dendritic Spines in Response to Repetitive Synaptic Input

EDWARD GAMBLE AND CHRISTOF KOCH*

Increased levels of intracellular calcium at either pre- or postsynaptic sites are thought to precede changes in synaptic strength. Thus, to induce long-term potentiation in the hippocampus, periods of intense synaptic stimulation would have to transiently raise the levels of cytosolic calcium at postsynaptic sites—dendritic spines in the majority of cases. Since direct experimental verification of this hypothesis is not possible at present, calcium levels have been studied by numerically solving the appropriate electro-diffusion equations for two different postsynaptic structures. Under the assumption that voltage-dependent calcium channels are present on dendritic spines, free intracellular calcium in spines can reach micromolar levels after as few as seven spikes in 20 milliseconds. Moreover, a short, but high-frequency, burst of presynaptic activity is more effective in raising levels of calcium and especially of the calcium-calmodulin complex than sustained low-frequency activity. This behavior is different from that seen at the soma of a typical vertebrate neuron.

AN INCREASE IN FREE, INTRACELLULAR calcium is believed to be the critical signal initiating the sequence of events leading to short- or long-term modifications of synaptic strength (1, 2). It has been proposed that the entry of calcium at the postsynaptic site triggers actin-myosin contractions in the spine neck (3), thereby inducing a change in the synaptic effective-

ness (4). In other proposals, calcium activates a proteinase, which can increase the number of glutamate receptors (2), reduce

Center for Biological Information Processing, Massachusetts Institute of Technology, Cambridge, MA 02139.

*To whom correspondence should be addressed at Divisions of Biology and Engineering and Applied Science, 216-76, California Institute of Technology, Pasadena, CA 91125.

potassium currents (5), or trigger a molecular switch by autophosphorylation of a protein kinase that could store information beyond the lifetime of any single protein (6). A critical feature of synaptic plasticity is its selectivity: only a certain class of signals—coded in the specific pattern of the presynaptic input—should modify synaptic strength while all other signals should not perturb the system. In the cortex, the majority of excitatory, postsynaptic sites are on dendritic spines. Their small spatial dimensions make them experimentally inaccessible; thus we have resorted to numerically solving the appropriate electrical and diffusion equations (7) of a typical mammalian pyramidal cell spine (8). We can then compare the calcium summation behavior in response to synaptic input with that expected at a typical vertebrate cell body, in this case type B bullfrog sympathetic ganglion cells.

The input to the spine is provided through an excitatory synapse and has the effect of transiently increasing the membrane conductance for Na^+ ions. This

change in conductance is triggered by a single or a train of regularly spaced presynaptic action potentials. In addition to these neurotransmitter-activated voltage-independent channels, the spine head membrane is assumed to contain a slow, noninactivating potassium current I_K , similar to that reported in hippocampal pyramidal cells (9), and a fast calcium current I_{Ca} , similar to that found in the hippocampus and in other locations (10). This calcium current is believed to underlie the high-threshold Ca^{2+} spikes most likely originating in the dendritic tree (11) and is assumed to become inactive with increased levels of intracellular calcium, $[\text{Ca}^{2+}]_i$. The detailed kinetics of both currents (see legend to Fig. 1) are taken from the description of similar currents in bullfrog ganglion cells, on the basis of extensive voltage clamp data (12). Also included in our model is a high-affinity, low-capacity, nonsaturable adenosine triphosphate (ATP)-driven calcium transport system, pumping free, intracellular Ca^{2+} into the extracellular matrix (13). Moreover, we have assumed that two nondiffusive calcium

buffering systems, calmodulin and calcineurin, are distributed throughout the spine. High concentrations of both buffers have been identified in postsynaptic structures and spines (14). The binding of calcium to calcineurin and to each of the four Ca^{2+} -specific binding sites at the calmodulin protein is governed by a first-order differential equation (15). We also included the effect of Ca^{2+} diffusing away from the submembrane space, into the spine head, through the neck, and ultimately into the dendrite. The appropriate equations were integrated numerically with a first-order Euler routine.

The membrane potential and the increase in calcium after a single synaptic input are shown in Fig. 2. Because of the high input impedance of the spine and its small membrane capacity, the synaptic input will induce a fast and large excitatory postsynaptic potential (EPSP), thereby activating even high-threshold calcium channels. In the submembrane compartment, calcium initially rushes in faster than it can be bound by the buffers, with the result being the typical biphasic change in calcium seen throughout the spine. After about 2 msec the calcium current terminates and the action of diffusion and—to a lesser extent—the action of the pump determine the subsequent slower decline in $[\text{Ca}^{2+}]_i$. The calcium concentration drops below $0.1 \mu\text{M}$ after 30 msec in the submembrane space and after 14 msec in the distal portion of the spine neck.

The trajectory of the potential and of $[\text{Ca}^{2+}]_i$ after intensive presynaptic activity is illustrated in Fig. 3. Note the increase in the potential after the first four spikes, as a result of summation of the EPSPs (Fig. 3A). Figure 3B shows the dynamics of calcium and of the calcium-calmodulin complex after ten spikes at different presynaptic firing frequencies. If all ten spikes occur within a burst lasting 30 msec, $[\text{Ca}^{2+}]_i$ in the neck rises to $1.44 \mu\text{M}$. The same number of presynaptic spikes at 100 and 50 Hz elevates calcium to only 0.47 and $0.31 \mu\text{M}$, respectively. Note that the firing frequency is never so high as to prevent most of the inflowing calcium from being buffered. Only for firing frequencies of 500 Hz and higher would calcium accumulation as a result of insufficient buffering play a significant role (see the time-course of $[\text{Ca}^{2+}]_i$ in Fig. 2). Our calculations did not show any saturation of the calcium buffers. The main reason for the nonlinear calcium summation is the small volume of spines. In conjunction with the fast kinetics of the buffer, the free calcium in spines comes essentially to equilibrium within 1 or 2 msec. Subsequently, the spine “loses” calcium through the calcium pump in the membrane and through the neck by diffusion into the dendrite where

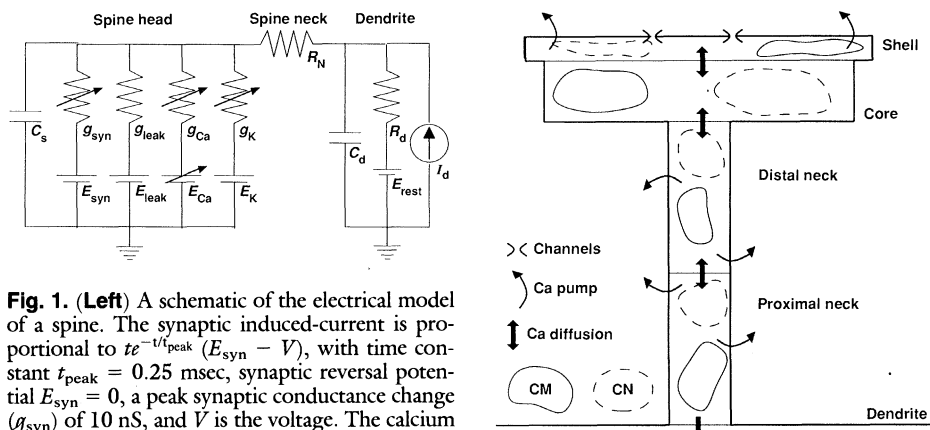


Fig. 1. (Left) A schematic of the electrical model of a spine. The synaptic induced-current is proportional to $te^{-t/\tau_{\text{peak}}}(E_{\text{syn}} - V)$, with time constant $\tau_{\text{peak}} = 0.25$ msec, synaptic reversal potential $E_{\text{syn}} = 0$, a peak synaptic conductance change (g_{syn}) of 10 nS, and V is the voltage. The calcium current is given by $I_{\text{Ca}} = \bar{g}_{\text{Ca}}m^2h(E_{\text{Ca}} - V)$, with peak calcium conductance $\bar{g}_{\text{Ca}} = 0.3$ nS, calcium potential $E_{\text{Ca}} = -12.5 \log([\text{Ca}^{2+}]_{\text{shell}}/[\text{Ca}^{2+}]_0)$ and $[\text{Ca}^{2+}]_0$ the constant, extracellular calcium concentration (2mM). The kinetics of this current are governed by the auxiliary equations $dm/dt = (m_{\infty} - m)/\tau_m$ with $m_{\infty} = (1 + e^{(3-V)/8})^{-1}$ and $\tau_m = 3.9/\cosh((V+6)/16)$ in milliseconds and $h = K/(K + [\text{Ca}^{2+}]_{\text{shell}})$ with the dissociation constant $K = 10 \mu\text{M}$. Thus, at $10 \mu\text{M}$ of intracellular free calcium, 50% of the calcium current is inactivated. At rest, the intracellular calcium concentration is 58 nM . The slow, noninactivating potassium current is given by $I_K = \bar{g}_K n(E_K - V)$, with peak potassium conductance $\bar{g}_K = 0.68$ nS and potassium potential $E_K = -86$ mV. The kinetics of the activation variable is governed by the equations $dn/dt = (n_{\infty} - n)/\tau_n$ with $n_{\infty} = (1 + e^{(-35-V)/10})^{-1}$ and $\tau_n = 152/\cosh((V+35)/20)$ in milliseconds. The parameters for the passive system are leakage conductance $g_{\text{leak}} = 28.6$ pS, leakage potential $E_{\text{leak}} = -70$ mV, spine head capacitance $C_s = 0.04$ pF, spine neck resistance $R_N = 175$ megohm, dendrite resistance $R_d = 400$ megohm, resting potential $E_{\text{rest}} = -75$ mV, and dendrite capacitance $C_d = 20$ pF. The input impedance is 560 megohm at the spine head and 390 megohm in the dendrite. (Right) A schematic of the calcium transport-buffering system in the spine. The shell compartment approximates a shell 50 nm thick just below the neuronal membrane. The remainder of the spine head is taken up by a spherical core of 250-nm radius. The spine neck, a thin cylinder 1.0 μm long and 0.05 μm in radius, is subdivided into two identical compartments. All compartments contain two stationary calcium buffering systems, calcineurin (CN) and calmodulin (CM). The shell contains $50 \mu\text{M}$ calmodulin and $10 \mu\text{M}$ calcineurin. All other compartments contain $25 \mu\text{M}$ calmodulin and $5 \mu\text{M}$ calcineurin. The forward binding rate and the dissociation rate for calcineurin are $0.05 \mu\text{M}^{-1} \text{msec}^{-1}$ and 0.025msec^{-1} , respectively. Calmodulin forms four calcium complexes. Our model assumes no cooperativity in binding between the four calcium binding sites and is based on $0.05 \mu\text{M}^{-1} \text{msec}^{-1}$ for the forward and 0.5msec^{-1} for the reverse rates of all complexes. The ATP-driven calcium extrusion pump is modeled by: $d[\text{Ca}^{2+}]_{\text{shell}}/dt = ([\text{Ca}^{2+}]_{\text{shell}} - C)/\tau_{\text{pump}}$, where $C = 50 \text{ nM}$ and $\tau_{\text{pump}} = 2$ msec. $[\text{Ca}^{2+}]$ in the dendrite remains constant at 58 nM , acting as a calcium sink. The discrete diffusion equations are solved with $D = 0.6 \mu\text{m}^2/\text{msec}$.

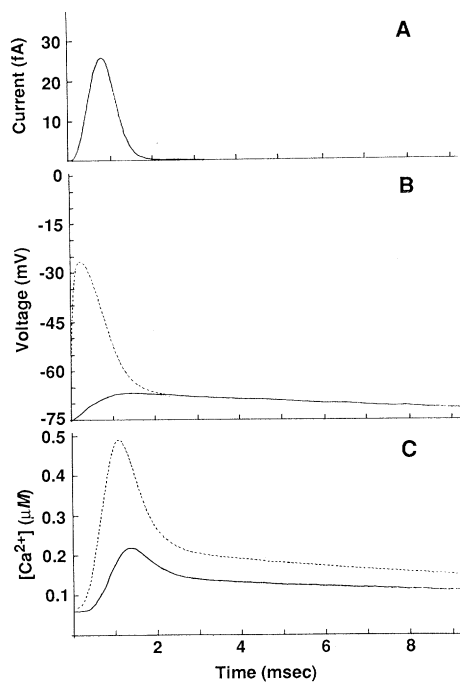


Fig. 2. (A) The time course of I_{Ca} , (B) the potential in the spine and in the dendrite (dotted and solid line, respectively), and (C) $[Ca^{2+}]_i$ in the submembrane space and in the distal neck (dotted and solid line, respectively), after a single synaptic input to the spine.

$[Ca^{2+}]_i$ will subside within a few micrometers to resting levels because of the large volume of the dendrite compared to the absolute amount of calcium leaving the spine and because of the presence of high-affinity buffers in the dendrite. For multiple presynaptic inputs, the decay of $[Ca^{2+}]_i$ is rapid: after about 250 msec, calcium levels are around 0.1 μM , regardless of the previous peak level of $[Ca^{2+}]_i$.

A much more dramatic effect can be observed if one considers the concentration of the fully bound calcium-calmodulin complex, $[Ca_4 \cdot CM]$. In the absence of any input, its resting level is very low: $3.3 \times 10^{-8} \mu M$. After ten presynaptic spikes at 333, 100, and 50 Hz, $[Ca_4 \cdot CM]$ in the neck increases to 4.5×10^{-3} , 4.4×10^{-5} , and $5.8 \times 10^{-6} \mu M$, respectively. Thus, small, experimentally almost undetectable, differences in the level of induced internal calcium can lead to much larger differences in the level of calcium binding proteins (Fig. 3B). This strongly nonlinear behavior is due to the fourth power relation between $[Ca_4 \cdot CM]$ and $[Ca^{2+}]_i$. Figure 3C reinforces these conclusions. Although an infinitely long train of spikes at 143 Hz will never increase levels of $[Ca^{2+}]_i$ above 1.0 μM , nor $[Ca_4 \cdot CM]$ above $0.5 \times 10^{-3} \mu M$, eight spikes at 333 Hz will drive $[Ca^{2+}]_i$ to 1.25 μM and $[Ca_4 \cdot CM]$ to $10^{-3} \mu M$.

The opposite calcium summation behav-

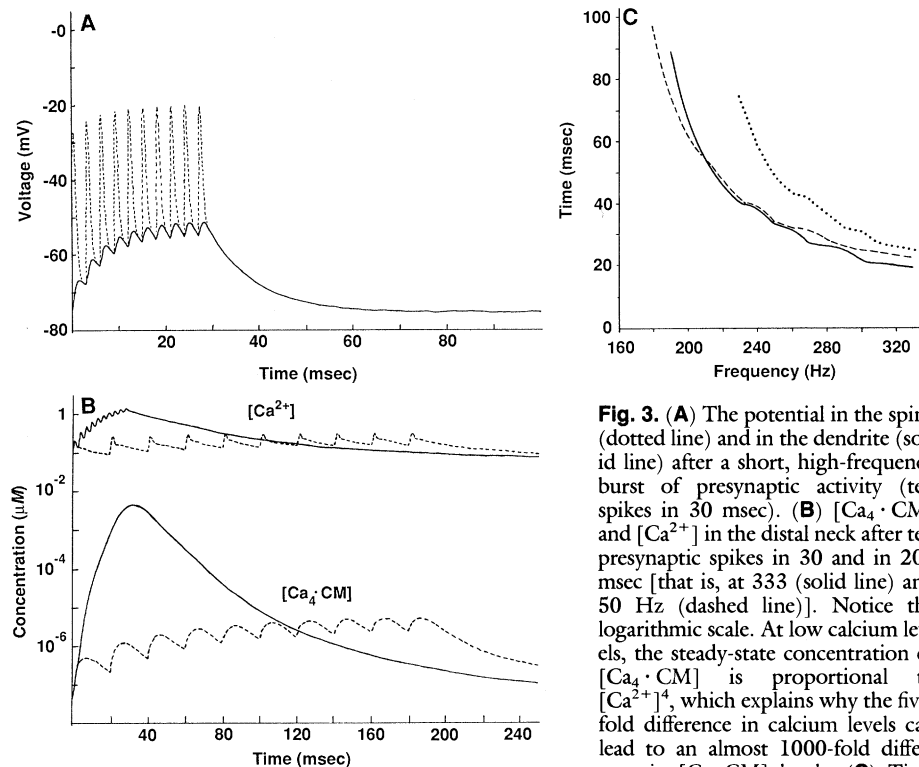


Fig. 3. (A) The potential in the spine (dotted line) and in the dendrite (solid line) after a short, high-frequency burst of presynaptic activity (ten spikes in 30 msec). (B) $[Ca_4 \cdot CM]$ and $[Ca^{2+}]_i$ in the distal neck after ten presynaptic spikes in 30 and in 200 msec [that is, at 333 (solid line) and 50 Hz (dashed line)]. Notice the logarithmic scale. At low calcium levels, the steady-state concentration of $[Ca_4 \cdot CM]$ is proportional to $[Ca^{2+}]_i^4$, which explains why the five-fold difference in calcium levels can lead to an almost 1000-fold difference in $[Ca_4 \cdot CM]$ levels. (C) Time required to reach a given level of $[Ca^{2+}]_i$ (solid lines, 1.0 μM ; dotted line, 1.25 μM) or $[Ca_4 \cdot CM]$ (dashed line, 1.0 nM) in the distal neck compartment for a given presynaptic firing frequency. In our standard model, input below about 180 Hz will fail to elevate calcium to these levels.

ior is observed in the cell body. Type B bullfrog sympathetic ganglion cell lack dendrites and have spherical cell bodies of about 20- μm radius. The electrical model of these cells includes seven types of channels, a single lumped calcium buffer, diffusion, an ATP-dependent calcium pump, and the nicotinic-induced synaptic EPSP (16). Figure 4 shows the calcium concentration throughout the inside of the cell after ten presynaptic spikes at different firing frequencies. Each EPSP triggers an action potential, activating I_{Ca} and leading to a small but constant (3 to 4 nM per spike) increase in $[Ca^{2+}]_i$, in good agreement with experimental data based on the use of the calcium dye arsenazo III (17). Because of the cell's large volume, calcium summation does not depend on the timing of the synaptic activity, but only on the absolute number of inputs (18).

But what happens to levels of intracellular calcium if a nearby excitatory synapse—on either a spine or a dendrite—is activated conjointly with the synapse on the spine? We have simulated this situation by injecting current into the dendrite just below the spine (see legend to Fig. 1A). At high presynaptic firing frequencies (333 Hz), the second synaptic input—firing at the same frequency—more than doubles the amount of free calcium in the spine neck; this enhancement is smaller at lower frequencies.

Figure 5 shows the maximal evoked change in $[Ca^{2+}]_i$ as a function of the relative phase between a 50-Hz input to the spine and a similar input to the dendrite. In other words, two separate but neighboring synaptic inputs firing at low frequency more than double the amount of evoked $[Ca^{2+}]_i$ if they fire out of phase. A similar phenomenon has recently been reported for the dentate gyrus (19).

What do these simulations imply for the biophysical mechanisms underlying synaptic plasticity? Elevated levels of cytosolic calcium seem to be required for the associative behavioral changes seen in mollusks (20) and for the establishment of long-term potentiation (LTP) (21), and can be observed after tetanic stimulation of hippocampal pyramidal cells (22). Our main result is that a short, high-frequency burst of spikes is more effective in elevating the concentration of free calcium in dendritic spines than longer spike trains of lower frequency (23). These high levels of $[Ca^{2+}]_i$ decay within hundreds of milliseconds, placing constraints on the temporal specificity of the calcium-dependent processes leading to an eventual establishment of LTP. The differences in calcium concentration are dramatically amplified when one considers the concentration of calcium-binding proteins (or enzymes), such as the calcium-calmodulin complex. This conclusion is to a large extent indepen-

dent of the specific parameters chosen for our model (24). Thus, short bursts of action potentials have special meaning for the nervous system, independent of their direct

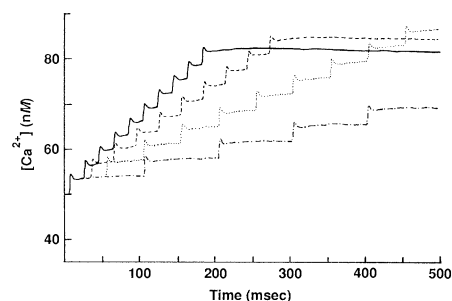


Fig. 4. The dynamics of $[Ca^{2+}]_i$ after ten synaptic inputs at different frequencies [50 (—), 33 (---), 20 (· · ·), and 10 Hz (- · -)] in simulated type B bullfrog sympathetic ganglion cells. Each nicotinic-induced EPSP ($t_{peak} = 2.5$ msec) triggers an action potential, activating I_{Ca} and leading to an influx of calcium. The calcium summation behavior is—to a first approximation— independent of the firing frequency. Thus, at all frequencies, the ten EPSPs raise $[Ca^{2+}]_i$ in the core compartment of the spherical cell (with a radius of 20 μm) to between 81 and 89 nM, in good agreement with experimental data (17). This model is based on extensive voltage-clamp data and includes seven time-, voltage-, and calcium-dependent important currents, a single lumped buffer, and three shells surrounding a well-mixed central core compartment (of 19- μm radius). It reproduces experimental results under a wide variety of different protocols, including both voltage and current clamp (16). The concentration of extracellular calcium is 4 mM.

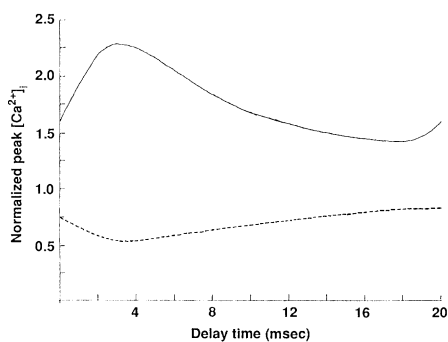


Fig. 5. Relative amount of maximal induced increase in $[Ca^{2+}]_i$ in the distal neck after application of a pair of simultaneous input pulse trains to both spine and dendrite (ten spikes at 50 Hz) as a function of the relative phase between both inputs. The current I_d induced by synaptic input to a neighboring spine is proportional to $te^{-t/t_{peak}}$ with $t_{peak} = 1$ msec to account for the low-pass filtering in the dendritic tree between the two spines (Fig. 1A). The upper curve illustrates the increase in the evoked calcium after depolarizing current injections to the dendrite, and the lower curve demonstrates a reduction in the evoked calcium concentration after hyperpolarizing current injections to the dendrite. In the absence of any synaptic input, the current injections caused a peak depolarization or hyperpolarization at the spine of +15 or -15 mV, respectively, relative to the resting potential.

effect on the postsynaptic potential, since they initiate cellular plasticity by means of the transient increase in $[Ca^{2+}]_i$. Accordingly, we expect that neurons which are prone to calcium-initiated changes in synaptic strength, for example, hippocampal pyramidal cells, receive bursty synaptic input, while less plastic neurons receive less or none. Such nonlinear calcium summation behavior does not occur in larger volumes, such as cell bodies or proximal dendrites, where each synaptic input evokes a small and constant increase in $[Ca^{2+}]_i$. In our model, I_{Ca} provides the link between synaptic inactivation and the increase in intracellular calcium. Other mechanisms for such a linkage are possible, for instance, a voltage- or calcium-dependent release of calcium from intracellular organelles (25), the sodium-calcium exchange pump working in reverse (26), or, in particular, the entry of calcium through activation of *N*-methyl-D-aspartic acid (NMDA) receptors by glutamate (27). We choose to simulate calcium entry with separate voltage-dependent calcium channels since not enough data are available to represent some of these other mechanisms and since NMDA receptors appear to be absent in the mossy fiber input to hippocampus CA3 pyramidal cells (28). Finally, we have shown how a second EPSP or IPSP (inhibitory postsynaptic potential), by acting on the voltage-dependent calcium channel, increases or decreases the amount of evoked calcium, commensurate with experimental data showing that LTP can be enhanced or prevented by combining synaptic activation with depolarizing or hyperpolarizing current injections (29). In other words, the postsynaptic potential serves as “liaison,” associating two or more spatially separate synaptic signals to each other by its effect on calcium influx. Ultimately, given the temporal and spatial constraint on intracellular communication, only voltage can link synaptic events to each other.

REFERENCES AND NOTES

1. E. R. Kandel, *Nature (London)* **293**, 697 (1981); D. L. Alkon, *Science* **226**, 1037 (1984).
2. G. Lynch and M. Baudry, *Science* **224**, 1057 (1984); J. C. Eccles, *Neuroscience* **10**, 1071 (1983).
3. F. Crick, *Trends Neurosci.* **5**, 44 (1982). This process would possibly operate via a calcium-activated calmodulin-dependent light chain kinase; see J. M. Scholey, K. A. Taylor, J. Kendrick-Jones *Nature (London)* **287**, 233 (1980).
4. W. Rall, in *Studies in Neurophysiology*, R. Porter, Ed. (Cambridge Univ. Press, Cambridge, 1978), pp. 203–209; C. Koch and T. Poggio, *Proc. R. Soc. London Ser. B* **218**, 455 (1983); G. M. Shepherd, R. K. Brayton, J. P. Miller, I. Segev, J. Rinzel, W. Rall, *Proc. Natl. Acad. Sci. U.S.A.* **82**, 2192 (1985); R. G. Coss and D. H. Perkel, *Behav. Neural Biol.* **44**, 151 (1985); F. Pongracz, *Neuroscience* **15**, 933 (1985); J. P. Miller, W. Rall, J. Rinzel, *Brain Res.* **325**, 325 (1985).
5. J. Acosta-Urquidí, D. L. Alkon, J. T. Neary, *Science*

- 224**, 1254 (1984); M. Sakakibara *et al.*, *Biophys. J.* **50**, 319 (1986).
6. F. Crick, *Nature (London)* **312**, 101 (1984); J. E. Lisman, *Proc. Natl. Acad. Sci. U.S.A.* **82**, 3055 (1985); S. Miller and M. B. Kennedy, *Cell* **44**, 861 (1986).
7. J. J. Jack, D. Noble, R. W. Tsien, *Electric Current Flow in Excitable Cells* (Clarendon, Oxford, 1975); N. Qian and T. J. Sejnowski, in *Cellular Mechanisms of Conditioning and Behavioral Plasticity*, C. W. Woody, D. L. Alkon, J. L. McGaugh, Eds. (Pergamon, London, in press).
8. For the geometry of spines on mammalian pyramidal cells, see L. E. Westrum and T. W. Blackstad, *J. Comp. Neurol.* **119**, 281 (1962); S. Jacobson, *ibid.* **129**, 49 (1967).
9. J. V. Halliwell and P. R. Adams, *Brain Res.* **250**, 71 (1982).
10. J. V. Halliwell, *J. Physiol. (London)* **341**, 10 (1983); P. R. Adams and M. Galvan, in *Advances in Neurology*, A. V. Delgado-Escueta, A. A. Ward, D. M. Woodbury, R. J. Porter, Eds. (Raven, New York, 1986), vol. 44, pp. 137–170.
11. H. Jahnsen and R. Llinas, *J. Physiol. (London)* **349**, 227 (1984).
12. P. R. Adams *et al.*, *J. Exp. Biol.* **124**, 259 (1986).
13. For our geometry and at $[Ca^{2+}]_i = 250$ nM, the calcium efflux due to the pump is 400 fmol $cm^{-2} sec^{-1}$; R. DiPolo and L. Beauge, *Annu. Rev. Physiol.* **45**, 313 (1983).
14. J. G. Wood, W. Wallace, J. N. Whitaker, W. Y. Cheung, *J. Cell Biol.* **84**, 66 (1980).
15. H. Rasmussen and P. Q. Barrett, *Physiol. Rev.* **64**, 938 (1984).
16. C. Koch and P. R. Adams, in preparation.
17. S. J. Smith, A. B. MacDermott, F. F. Weight, *Nature (London)* **304**, 350 (1983).
18. If the spine head is approximated by a sphere of radius 0.5 μm , the time for free calcium to reach equilibrium after synaptic induced calcium influx in the shell is about 1600 times longer in the cell body (of radius 20.0 μm) than in the spine. Since the decrease in $[Ca^{2+}]_i$ in the cell body (as a result of the calcium pump) is about 1 nM sec^{-1} , and about 150 nM $msec^{-1}$ in the proximal spine neck (as a result of diffusion into the dendrite), the accumulation of calcium after synaptic input occurs at two very different time scales in the two systems.
19. J. Winson and D. Dahl, *Science* **234**, 985 (1986).
20. D. L. Alkon and M. Sakakibara, *Biophys. J.* **48**, 983 (1985).
21. See, for instance, R. W. Turner, K. G. Baimbridge, J. J. Miller, *Neuroscience* **7**, 1411 (1982); G. Lynch, J. Larson, S. Kelso, G. Barrionuevo, F. Schottler, *Nature (London)* **305**, 719 (1983).
22. K. Krnjević, M. E. Morris, N. Ropert, *Brain Res.* **374**, 1 (1986).
23. H. Robinson and C. Koch, *Artificial Intelligence Lab. Memo No. 779* (Massachusetts Institute of Technology, Cambridge, MA, 1984).
24. The maximal evoked change in cytosolic calcium in the distal neck after a single spike is 0.218 μM for our standard parameter set (see legend to Fig. 1). A value for g_{Ca} of 0.03 or 0.6 nS changed the peak $[Ca^{2+}]_i$ to 0.08 or 0.36 μM , respectively; a value for t_{peak} of 0.125 or 0.5 msec changed the peak $[Ca^{2+}]_i$ to 0.10 or 0.60 μM , respectively; a value for peak synaptic conductance change of 5.0 or 20.0 nS changed the peak $[Ca^{2+}]_i$ to 0.10 or 0.48 μM , respectively; removal of the potassium channel or a value for g_K of 13.6 nS changed the peak $[Ca^{2+}]_i$ to 0.22 or 0.20 μM , respectively; a value for τ_{pump} of 20.0 or 0.2 msec changed peak $[Ca^{2+}]_i$ to 0.24 or to 0.11 μM , respectively; a change in the buffer dynamics by a factor of 0.2 or 5.0 changed the peak $[Ca^{2+}]_i$ to 0.38 or 0.12 μM , respectively; a change in the concentration of all buffers by a factor 0.5 or 2.0 changed the peak $[Ca^{2+}]_i$ to 0.30 or 0.14 μM , respectively; removal of all calcineurin increased peak $[Ca^{2+}]_i$ to 0.24 μM , and removal of all calcium inactivation increased peak $[Ca^{2+}]_i$ to 0.223 μM . For all these parameter changes, the shape of the nonlinear $[Ca^{2+}]_i$ and $[Ca_a \cdot CM]$ summation curves (Fig. 3B) remain unchanged with the exception of $g_{Ca} = 0.03$ nS, $t_{peak} = 0.125$ msec, or $\tau_{pump} = 0.2$ msec. In these cases the differences in summation behavior for low- and high-frequency activity was less pronounced. Thus, although the total amount of inflowing calcium after a single synaptic event can vary significantly, our conclusions remain valid.
25. Such as the spine apparatus where calcium has been reported; E. Fikova, A. J. Markham, R. J. Delay, *Brain Res.* **266**, 163 (1983).

26. P. F. Baker and P. A. McNaughton, *J. Physiol. (London)* **260**, 24 (1976).
27. R. Dingleline, *ibid.* **343**, 385 (1983); A. B. McDermott *et al.*, *Nature (London)* **321**, 519 (1986).
28. D. T. Monaghan and C. W. Cotman, *J. Neurosci.* **5**, 2909 (1985). Moreover, NMDA antagonists do not block LTP of the mossy fiber synaptic input to CA3 cells [E. W. Harris, and C. W. Cotman, *Neurosci. Lett.* **70**, 132 (1986)].
29. G. Barriounevo and T. H. Brown, *Proc. Natl. Acad. Sci. U.S.A.* **80**, 7347 (1983); H. Wigstrom, B. Gustafsson, Y.-Y. Huang, W. C. Abraham, *Acta Physiol. Scand.* **126**, 317 (1986); R. Malinow and J. P. Miller, *Nature (London)* **320**, 529 (1986); S. R. Kelso, A. H. Ganang, T. H. Brown, *Proc. Natl. Acad. Sci. U.S.A.* **83**, 5326 (1986).
30. This research has profited from many discussions with H. Robinson of the Physiological Laboratory in Cambridge, England. E.G. was supported by a Fairchild Fellowship and C.K. by a grant from the Office of Naval Research, Engineering Psychology Division awarded to T. Poggio and in part by the

National Science Foundation under grant PHY82-17853, supplemented by funds from the National Aeronautics and Space Administration. We thank H. Lester for critically reading the manuscript and both the Artificial Intelligence Laboratory at the Massachusetts Institute of Technology and the Institute of Theoretical Physics at the University of California at Santa Barbara for the kind use of their facilities.

9 December 1986; accepted 7 April 1987

The Role of Individual Cysteine Residues in the Structure and Function of the *v-sis* Gene Product

N. A. GIESE, K. C. ROBBINS, S. A. AARONSON

The *v-sis* oncogene encodes a platelet-derived growth factor (PDGF)-related product whose transforming activity is mediated by its functional interaction with the PDGF receptor. PDGF, as well as processed forms of the *v-sis* gene product, is a disulfide-linked dimer with eight conserved cysteine residues in the minimum region necessary for biologic activity. Site-directed mutagenesis of the *v-sis* gene revealed that each conserved cysteine residue was required directly or indirectly for disulfide-linked dimer formation. However, substitution of serine for cysteine codons at any of four positions had no detrimental effect on transforming activity of the encoded *v-sis* protein. These results establish that interchain disulfide bonds are not essential in order for this protein to act as a functional ligand for the PDGF receptor. The remaining four substitutions of serine for cysteine each inactivated transforming function of the molecule. In each case this was associated with loss of a conformation shown to involve intramolecular disulfide bonds. These studies provide insight into the role of individual cysteine residues in determining the structure of the *sis*/PDGF molecule critical for biological activity.

THE PRODUCT OF THE SIMIAN SARCOMA virus (SSV) transforming gene, *v-sis*, exhibits all of the known structural and functional properties of human platelet-derived growth factor (PDGF), a potent mitogen for connective tissue cells (1-4). Moreover, *v-sis* alters growth properties only of cells that express PDGF receptors (4), implying that the transforming activity of *v-sis* is mediated directly by interaction of its PDGF-like

product with the PDGF receptor. Since the minimal region of the *v-sis* gene product required for transforming activity is homologous to one of the two peptide chains comprising PDGF (5-7), genetic manipulations of *v-sis* that impair its transforming function provide a means of studying the ability of both its products and PDGF to act as ligands for the PDGF receptor.

PDGF as well as processed forms of the *v-sis* product are disulfide-linked dimers,

whose mitogenic activities are abolished upon reduction (8-10). Despite evolutionary divergence (1, 2), PDGF-1, PDGF-2, and the *v-sis* product, which is the monkey homologue of PDGF-2, all contain eight identically spaced cysteine residues within a core sequence required for biological activity. In *v-sis* (Fig. 1), the core region contains 84 codons; five of the eight cysteines are clustered in a span of only 18 residues (amino acids 154 to 171). In the present study, we have investigated the role of individual cysteine residues on the structure and function of the *v-sis* transforming protein.

Genetic manipulations of *v-sis* were accomplished by site-directed mutagenesis. A 1.2-kbp fragment containing *v-sis* was removed from the pSSVSV2 plasmid (5) and subcloned into M13mp19. By means of a 17-mer oligonucleotide with the appropriate mismatch, a serine codon was substituted for each cysteine codon according to the methods of Zoller and Smith (11) as modified by Kunkel to allow for phenotypic selection of phage containing the desired mutation (12). Mutants were identified and their DNA sequences verified by the dideoxynucleotide method (13). Each mutant *v-sis* was then transferred back into pSSVSV2 for analysis of biological activity upon transfection of NIH 3T3 cells. Since the plasmid vector containing the *v-sis* mutants also had a dominant selectable *gpt* marker gene, it was possible to score focus-forming activity as well as colony formation for each plasmid.

Four of the eight mutants demonstrated transforming activities equivalent to that of wild-type SSV, whereas the other four mutants lacked any detectable transforming activity (Table 1). Each of the eight constructs was fully active with respect to the induction of colony formation in HAT (hypoxanthine, aminopterin, thymidine) medium. These results established that cysteine residues 127, 160, 171, and 208 were essential for *v-sis* transforming activity, whereas the loss of any one of the remaining cysteines had no

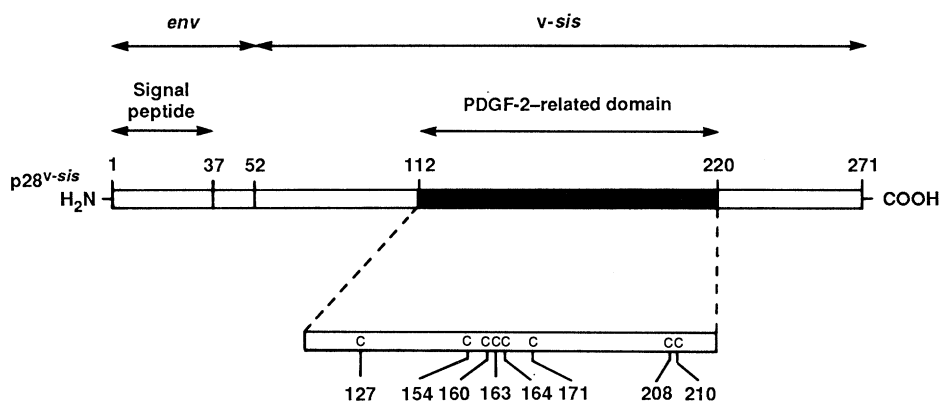


Fig. 1. Structural features of p28^{v-sis} and distribution of cysteine residues within its PDGF-2-related domain. The initiation codon for p28^{v-sis} synthesis is assigned position 1. The region spanning residues 1 through 51 is derived from the simian sarcoma-associated virus *env* gene, and residues 1 through 36 represent the p28^{v-sis} signal peptide. The region that is homologous to human PDGF-2 spans residues 112 through 220.

Laboratory of Cellular and Molecular Biology, National Cancer Institute, National Institutes of Health, Bethesda, MD 20892.